

## Calculation of Heat Transfer and Fluid Flow in Complex Geometries Using a Finite Volume Method in Body-Fitted Coordinates

**Putivisutisak S.**

*Department of Mechanical Engineering, Faculty of Engineering, Chulalongkorn University, Bangkok, Thailand*

*E-mail address: sompong.pu@chula.ac.th*

**Prasertlarp S.**

*Department of Mechanical Engineering, Faculty of Engineering, Chulalongkorn University, Bangkok, Thailand*

### **Abstract**

*Heat transfer and fluid flows in various complicated geometries are numerically investigated using a finite volume method. The computation is based on a body-fitted coordinate system on a staggered grid with Cartesian velocity components as the dependent variables. The transfinite interpolation (TFI) is used to generate the initial grid and the elliptic grid generation technique is employed to adjust the grid smoothness. The SIMPLE algorithm is utilized for the pressure-velocity coupling. The flows of interest are laminar, steady and incompressible. A case of heat diffusion and two cases of internal flows are considered here; heat conduction in a square plate with a circular hole, flows through a gradual-expansion channel, and a channel with wavy wall. The results are compared with analytical or numerical data available in the literature. It can be seen that the present method can accurately solve heat transfer and fluid flow problems in complex geometries.*

**Keywords:** *Finite volume method, Body-fitted coordinates, Complex geometries*

### **1 Introduction**

Finite volume method has been a widely used numerical tool to solve heat transfer and fluid flow problems. It gains popularity because of its physically conservative nature, simplicity and suitability for solving strongly nonlinear governing equations. However, a major limitation of the traditional finite volume method is the incapability to solve problems in complex domain.

The trouble can be removed by applying the method with a generalized coordinate system, so-called body-fitted coordinates. Unlike the conventional rectangular coordinate systems such as Cartesian, cylindrical or spherical coordinates, the body-fitted coordinates do not have fixed directions, thus allowing easy and accurate implementation of boundary conditions of the heat transfer and flow in complex geometry.

Among first pioneers in the field of calculation in the body-fitted coordinates are Vinokur [1], Thompson et al. [2-5], Gordon and Hall [6] and Vanka et al. [7]. Over the years, the grid generation techniques have been developed continuously and various velocity components were chosen as the dependent variables to improve the computation accuracy. The merits in choosing different velocity components as the dependent variables were extensively discussed in Karki [8] and Melaaen [9].

Finite volume method based on the body-fitted coordinates has been employed in many computational fluid dynamics researches. Among the outstanding and most being cited works are Peric [10], Shyy et al. [11] and Karki and Patankar [12].

Presently, since most engineering heat and fluid flow problems take place in irregular geometries, the

method has been held as a practical solution for dealing with such problems. Recent works includes Talukdar et al. [13], Oztop [14], Mohammed et al. [15], Piller and Stalio [16] and Baghlani [17], among others.

This paper presents a finite volume method for solving steady two-dimensional heat diffusion and laminar flow in complex geometries. The computation is based on a body-fitted coordinate system on a staggered grid with Cartesian velocity components as the dependent variables. For simplicity, the first-order upwind scheme is utilized for approximating the convected values at control volume faces. The pressure field is calculated using SIMPLE algorithm [18]. For the grid generation part, the initial grid is generated by the transfinite interpolation (TFI) and then the grid smoothness is adjusted by the elliptic grid generation technique using Poisson equation.

The developed computer program is validated with simple problems, of which analytical solutions or other numerical results are available. The test cases are heat diffusion in a square plate with a circular hole, flow in gradual-expansion channel and flow past a wavy wall channel.

## 2 Grid generation

A grid generator is employed to distribute the grid lines dividing domains into control volumes. The present work uses the TFI to generate the initial grid and then the elliptic grid generation technique using Poisson equation to adjust the grid smoothness (details were discussed in Porameesanaporn [19]).

The method of TFI distributes points on boundaries to generate the grid points inside the physical domain by interpolation. Particular formulations of the TFI method allow for angle and grid spacing control at the boundaries. From linear Lagrange interpolation functions, the grid coordinate can be generated by

$$r(\xi, \eta) = \sum_{n=1}^2 \phi_n \left( \frac{\xi}{I} \right) r(\xi_n, \eta) + \sum_{m=1}^2 \psi_m \left( \frac{\eta}{J} \right) r(\xi, \eta_m) - \sum_{n=1}^2 \sum_{m=1}^2 \phi_n \left( \frac{\xi}{I} \right) \psi_m \left( \frac{\eta}{J} \right) r(\xi_n, \eta_m) \quad (1)$$

where  $I$  and  $J$  are the maximum values of  $\xi$  and  $\eta$ , respectively. The functions  $\phi_n$  and  $\psi_m$  can be selected as linear functions as follows

$$\phi_1 \left( \frac{\xi}{I} \right) = 1 - \frac{\xi}{I}, \quad \phi_2 \left( \frac{\xi}{I} \right) = \frac{\xi}{I} \quad (2)$$

$$\psi_1 \left( \frac{\eta}{J} \right) = 1 - \frac{\eta}{J}, \quad \psi_2 \left( \frac{\eta}{J} \right) = \frac{\eta}{J} \quad (3)$$

An elliptic grid is obtained by solving a set of partial differential equations. The basic idea comes from Poisson equation

$$\frac{\partial^2 \xi_i}{\partial x_i^2} = P_i \quad (4)$$

Using chain rule, the relation for the coordinate transformation is obtained from

$$\begin{bmatrix} \frac{\partial \xi}{\partial x} & \frac{\partial \eta}{\partial x} \\ \frac{\partial \xi}{\partial y} & \frac{\partial \eta}{\partial y} \end{bmatrix} = \frac{1}{J} \begin{bmatrix} \frac{\partial y}{\partial \eta} & -\frac{\partial y}{\partial \xi} \\ -\frac{\partial x}{\partial \eta} & \frac{\partial x}{\partial \xi} \end{bmatrix} \quad (5)$$

where  $J$  is the Jacobian which is given by

$$J = \frac{\partial x}{\partial \xi} \frac{\partial y}{\partial \eta} - \frac{\partial x}{\partial \eta} \frac{\partial y}{\partial \xi} \quad (6)$$

Substituting those values into Poisson equation, the partial differential equations for grid generation are obtained as shown

$$\alpha \frac{\partial^2 x}{\partial \xi^2} - 2\beta \frac{\partial^2 x}{\partial \xi \partial \eta} + \gamma \frac{\partial^2 x}{\partial \eta^2} = -J^2 \left( P \frac{\partial x}{\partial \xi} + Q \frac{\partial x}{\partial \eta} \right) \quad (7)$$

$$\alpha \frac{\partial^2 y}{\partial \xi^2} - 2\beta \frac{\partial^2 y}{\partial \xi \partial \eta} + \gamma \frac{\partial^2 y}{\partial \eta^2} = -J^2 \left( P \frac{\partial y}{\partial \xi} + Q \frac{\partial y}{\partial \eta} \right) \quad (8)$$

where  $\alpha$ ,  $\beta$  and  $\gamma$  are

$$\alpha = \left( \frac{\partial y}{\partial \eta} \right)^2 + \left( \frac{\partial x}{\partial \eta} \right)^2 \quad (9)$$

$$\beta = \frac{\partial y}{\partial \eta} \frac{\partial y}{\partial \xi} + \frac{\partial x}{\partial \eta} \frac{\partial x}{\partial \xi} \quad (10)$$

$$\gamma = \left( \frac{\partial x}{\partial \xi} \right)^2 + \left( \frac{\partial y}{\partial \xi} \right)^2 \quad (11)$$

### 3 Governing equations

The governing equations in the body-fitted coordinates employed here can be presented as the following.

#### 3.1 Heat conduction

The governing equation for steady two-dimensional heat conduction in Cartesian coordinates is given as

$$\frac{\partial}{\partial x} \left( k \frac{\partial T}{\partial x} \right) + \frac{\partial}{\partial y} \left( k \frac{\partial T}{\partial y} \right) = 0 \quad (12)$$

Using the relation in Equation (5), the transformed governing equation is obtained as

$$\frac{\partial}{\partial \xi} \left[ \frac{k\alpha}{J} \frac{\partial T}{\partial \xi} - \frac{k\beta}{J} \frac{\partial T}{\partial \eta} \right] + \frac{\partial}{\partial \eta} \left[ \frac{k\gamma}{J} \frac{\partial T}{\partial \eta} - \frac{k\beta}{J} \frac{\partial T}{\partial \xi} \right] = 0 \quad (13)$$

#### 3.2 Fluid flow

Governing equations for steady two-dimensional laminar flow in Cartesian coordinates can be shown as follows

Continuity:

$$\frac{\partial(\rho u)}{\partial x} + \frac{\partial(\rho v)}{\partial y} = 0 \quad (14)$$

Conservation of momentum:

$$\frac{\partial(\rho u u)}{\partial x} + \frac{\partial(\rho v u)}{\partial y} = \frac{\partial}{\partial x} \left( \mu \frac{\partial u}{\partial x} \right) + \frac{\partial}{\partial y} \left( \mu \frac{\partial u}{\partial y} \right) - \frac{\partial p}{\partial x} + S_u \quad (15)$$

$$\frac{\partial(\rho u v)}{\partial x} + \frac{\partial(\rho v v)}{\partial y} = \frac{\partial}{\partial x} \left( \mu \frac{\partial v}{\partial x} \right) + \frac{\partial}{\partial y} \left( \mu \frac{\partial v}{\partial y} \right) - \frac{\partial p}{\partial y} + S_v \quad (16)$$

Using the relation in Equation (5), the governing equations can be transformed as

Continuity:

$$\frac{\partial}{\partial \xi} \left( (\rho u) \frac{\partial y}{\partial \eta} - (\rho v) \frac{\partial x}{\partial \eta} \right) + \frac{\partial}{\partial \eta} \left( (\rho v) \frac{\partial x}{\partial \xi} - (\rho u) \frac{\partial y}{\partial \xi} \right) = 0 \quad (17)$$

Conservation of momentum:

$$\left[ \frac{\partial}{\partial \xi} \left( (\rho u u) \frac{\partial y}{\partial \eta} - (\rho v u) \frac{\partial x}{\partial \eta} \right) + \frac{\partial}{\partial \eta} \left( (\rho v u) \frac{\partial x}{\partial \xi} - (\rho u u) \frac{\partial y}{\partial \xi} \right) \right] \\ = \frac{\partial}{\partial \xi} \left( \frac{\mu \alpha}{J} \frac{\partial u}{\partial \xi} - \frac{\mu \beta}{J} \frac{\partial u}{\partial \eta} \right) + \frac{\partial}{\partial \eta} \left( \frac{\mu \gamma}{J} \frac{\partial u}{\partial \eta} - \frac{\mu \beta}{J} \frac{\partial u}{\partial \xi} \right) \\ - \left( \frac{\partial p}{\partial \xi} \frac{\partial y}{\partial \eta} \right) + \left( \frac{\partial p}{\partial \eta} \frac{\partial y}{\partial \xi} \right) + JS_u \quad (18)$$

$$\left[ \frac{\partial}{\partial \xi} \left( (\rho u v) \frac{\partial y}{\partial \eta} - (\rho v v) \frac{\partial x}{\partial \eta} \right) + \frac{\partial}{\partial \eta} \left( (\rho v v) \frac{\partial x}{\partial \xi} - (\rho u v) \frac{\partial y}{\partial \xi} \right) \right] \\ = \frac{\partial}{\partial \xi} \left( \frac{\mu \alpha}{J} \frac{\partial v}{\partial \xi} - \frac{\mu \beta}{J} \frac{\partial v}{\partial \eta} \right) + \frac{\partial}{\partial \eta} \left( \frac{\mu \gamma}{J} \frac{\partial v}{\partial \eta} - \frac{\mu \beta}{J} \frac{\partial v}{\partial \xi} \right) \\ - \left( \frac{\partial p}{\partial \xi} \frac{\partial x}{\partial \eta} \right) + \left( \frac{\partial p}{\partial \eta} \frac{\partial x}{\partial \xi} \right) + JS_v \quad (19)$$

The values of  $\alpha$ ,  $\beta$  and  $\gamma$  are as shown in Equations (9) – (11). Details of the transformation technique and discretization method can be found in Putivisutisak [20].

### 4 Physical models

There are three test cases being utilized for computer code validation here, i.e. heat diffusion in a square plate with a circular hole, flow in gradual-expansion channel and flow past a wavy wall channel. Details of their physical models are given as the following.

#### 4.1 Square plate with a circular hole

The geometry of the square plate with a circular hole is shown in Figure 1. The temperatures at the inner circular and outer square surfaces are  $T_1$  and  $T_2$ , respectively. The solution for the heat transfer rate can be obtained using the graphical method [21] as

$$q = Sk(T_1 - T_2) \quad (20)$$

where  $S$  is the shape factor calculated from

$$S = \frac{2\pi L}{\ln(1.08 w/D)} \quad (21)$$

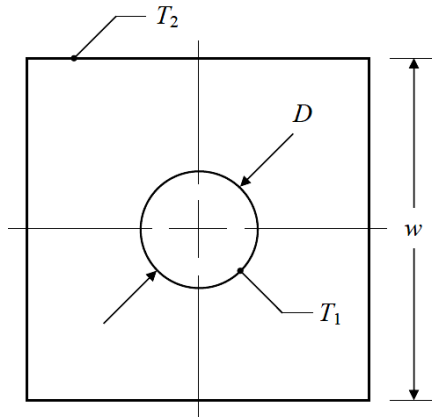


Figure 1: Geometry of square plate with a circular hole.

### 4.2 Gradual-expansion channel

The gradual-expansion channel geometry is shown in Figure 2. The curvature at the top of the channel is determined by the Reynolds number,  $Re$ , with the channel height ( $y_w$ ) being calculated from Equation (22). The length of the channel is equal to  $Re/3$ .

$$y_w = 1 - 0.5 \left[ \tanh \left( 2 - 30 \frac{x}{Re} \right) - \tanh(2) \right], 0 \leq x \leq \frac{Re}{3} \quad (22)$$

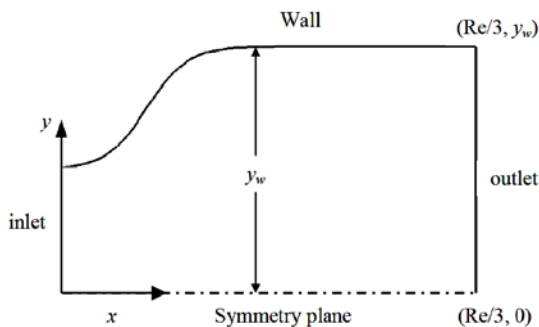


Figure 2: Geometry of Gradual-expansion channel.

The boundary conditions are as follows

- inlet: fully developed flow with the velocities given as

$$u = \frac{3}{2} (y_{\max}^2 - y^2), \quad v = 0 \quad (23)$$

- outlet: fully developed flow
- top: wall
- bottom: symmetry plane

### 4.3 Wavy wall channel

The third test case is laminar flow through a wavy wall channel. The channel geometry is shown in Figure 3. The wavy wall part is between the location  $x = 3$  to  $x = 15$ . Other than that, the channel is direct. The wavy wall consists of six continuous waves and its characteristic is given as

$$y = 1 + a \cdot \sin((x - 3)\pi), \quad 3 \leq x \leq 15 \quad (24)$$

where  $a$  is the amplitude of the wave.

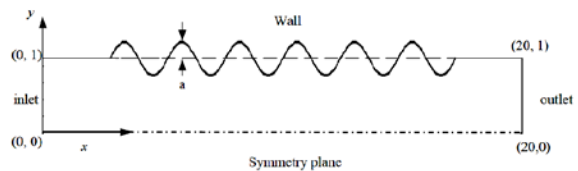


Figure 3: Geometry wavy wall channel (not to scale)

The boundary conditions are similar to those in the case of flow through gradual-expansion channel.

## 5 Result and discussion

### 5.1 Square plate with a circular hole

For the heat diffusion problem in the square plate with a circular hole, the circle diameter,  $D = 2$  cm; square width,  $w = 4$  cm; plate depth,  $L = 1$  m; thermal conductivity,  $k = 100$  W/cm · K and inner and outer temperatures,  $T_1$  and  $T_2$  are 100 and 0°C, respectively. Substituting these values into Equations (20) and (21) yields the heat transfer rate of 815.8 W.

Due to symmetry, only one-fourth of the plate is considered. Figure 4 shows a typical grid layout of the plate. Grid independence test is done with grid sizes of 18x8, 67x28 and 100x42. It is found that grid independent results can be obtained from the 67x28 grid size. Temperature distribution is presented in Figure 5. The numerical heat transfer rate is 816.2 W. It can be seen that the result differs from that of the graphical method only around 0.05%.

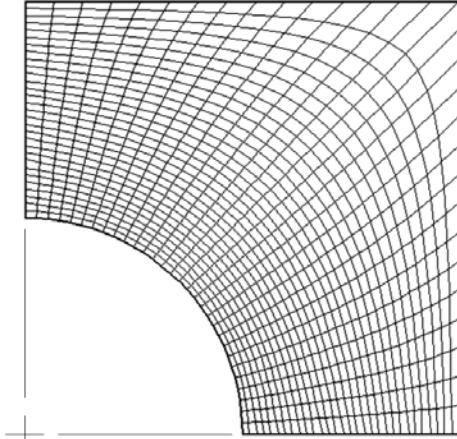


**Figure 4:** Square plate with a circular hole; Typical grid of 30x30.

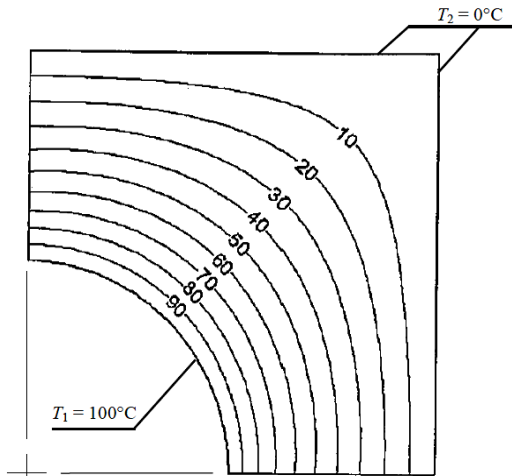


**Figure 5:** Square plate with a circular hole; Temperature distribution.

### 5.2 Gradual-expansion channel

In this case, comparison is made with the benchmark by Cliffe et al. [22] which uses the finite element method for the calculation. The numerical grid is shown in Figure 6. The Reynolds number of the flow is 10. Grid independence test is made by computing the pressure in the channel, with grid sizes of 22x22, 42x42 and 62x62. It is seen that the 42x42 grid is sufficiently fine enough to give a grid independent result.

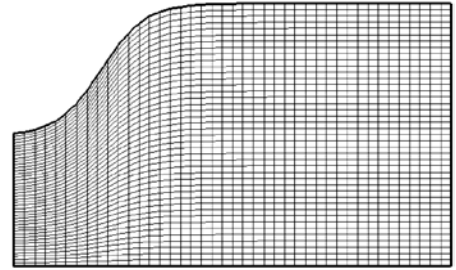


**Figure 6:** Gradual-expansion channel; Numerical grid of 42x42.

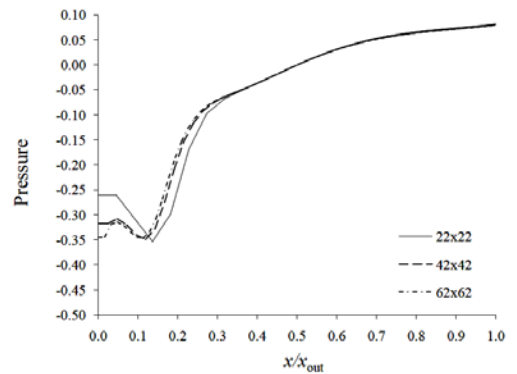


**Figure 7:** Gradual-expansion channel; Pressure distribution for different grid sizes.

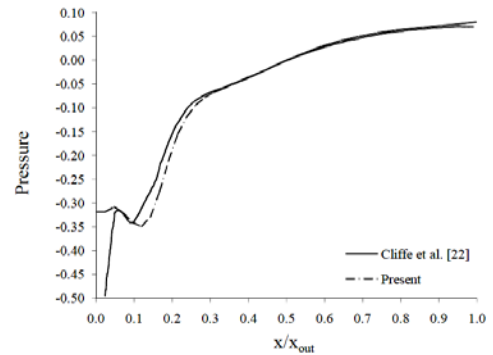


**Figure 8:** Gradual-expansion channel; Pressure distribution.

Figure 8 shows the comparison of the pressure throughout the domain between the present simulation and the calculation of Cliffe et al. [22]. The results for the initial part of the channel are moderately different from the benchmark. Some researchers had experienced a similar difference.

Burn and Wilkes [23] had reasoned that the difference was caused from the the fully developed flow boundary condition at the sloped entrance. In addition, the domain length is not long enough for the flow to be fully developed at the exit. Melaaen [9] had found that the pressure gradients at the entrance were very high, as shown in Figure 9. As a result, very large number of grid near the entrance may be required to yield a similar result to the benchmark. Nevertheless, the calculated pressure for the rest of the channel agrees well with Cliffe et al. [22].

Figures 9 and 10 illustrate the pressure distribution and streamlines, respectively. It can be seen from these qualitative comparison that the results are well consistent with the calculation of Melaaen [9].

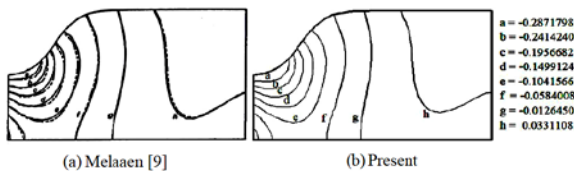


Figure 9: Gradual-expansion channel; Pressure distribution.

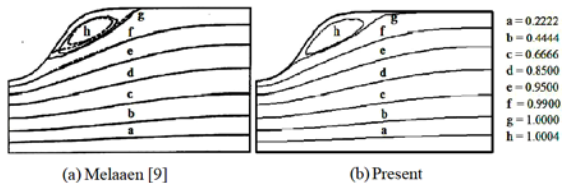


Figure 10: Gradual-expansion channel; Streamlines.

### 5.3 Wavy wall channel

Validation in this case is made using the product  $ReC_f$  for the entire length of the domain, where  $C_f$  is the friction coefficient at the wall which is calculated from

$$C_f = \frac{\tau}{\rho u^2} \quad (25)$$

where  $\tau$  is the shear force given by

$$\tau = \mu \left( \frac{\partial u}{\partial y} + \frac{\partial v}{\partial x} \right)_{y=y_w} \quad (26)$$

The calculation is made at  $Re = 100, 300$  and  $500$ , where the amplitude ( $a$ ) of the wall is  $0.1$  and  $0.2$ . Figure 11 presents the grid independence test using friction coefficient results from three grid sizes. It may be seen that the results from the  $180 \times 20$  grid differ only slightly from those of the  $270 \times 30$  grid. Hence, it may be assumed that the  $180 \times 20$  grid gives the grid independent results.

The numerical results are compared with results from a finite difference method by Wang and Chen [24], as shown in Figures 12 – 15. It can be seen that fairly good agreement is achieved for all cases.

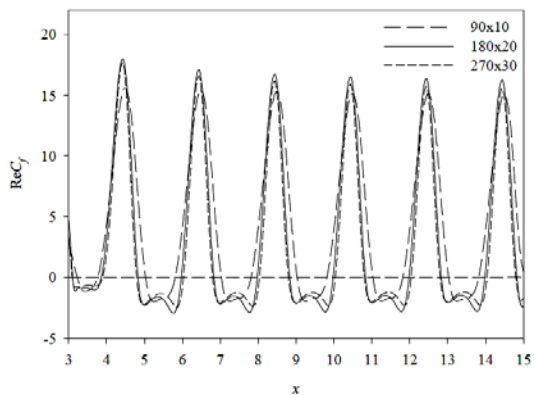


Figure 11: Wavy wall; Comparison of friction coefficient distribution for different grid sizes ( $Re = 500$  and  $a = 0.2$ ).

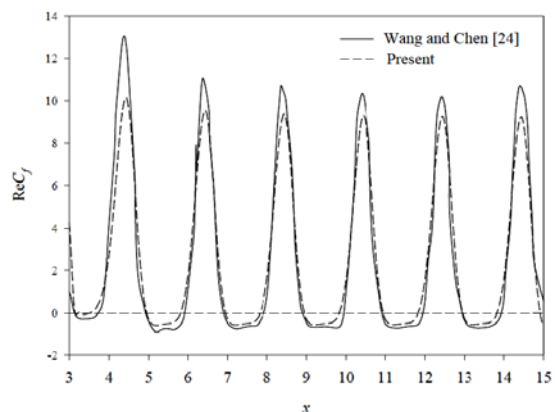
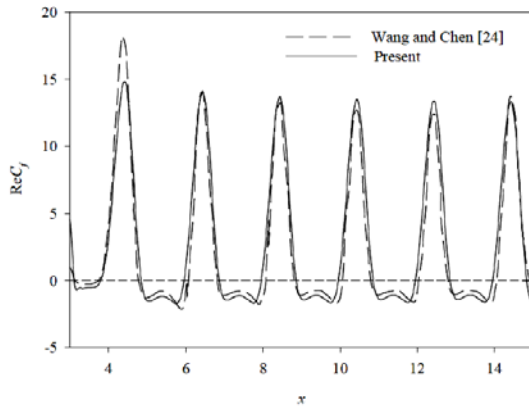
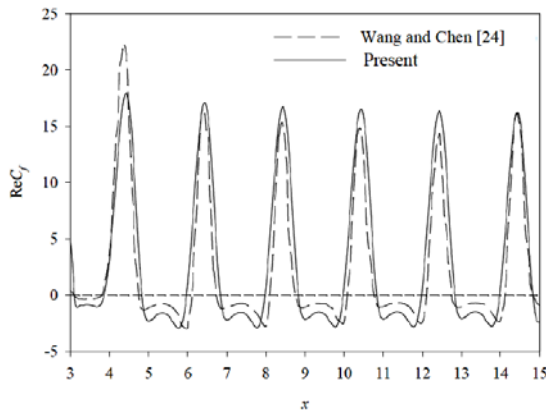


Figure 12: Wavy wall; Friction coefficient distribution at wall ( $Re = 100$  and  $a = 0.2$ ).



**Figure 13:** Wavy wall; Friction coefficient distribution at wall (Re = 300 and  $a = 0.2$ ).



**Figure 14:** Wavy wall; Friction coefficient distribution at wall (Re = 500 and  $a = 0.2$ ).

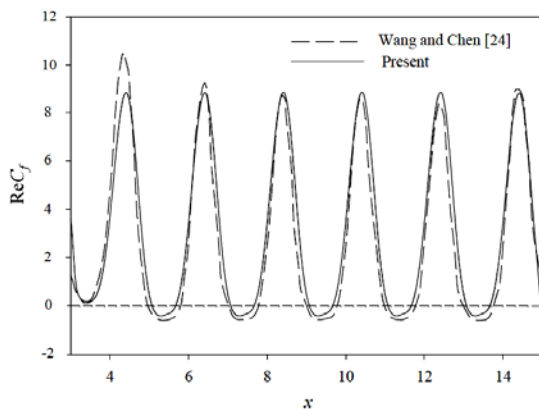


**Figure 15:** Wavy wall; Friction coefficient distribution at wall (Re = 500 and  $a = 0.1$ ).

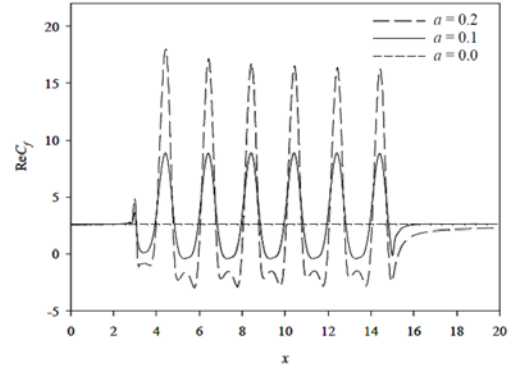


**Figure 16:** Wavy wall; Distribution of Friction coefficient with different amplitudes for Re = 500.

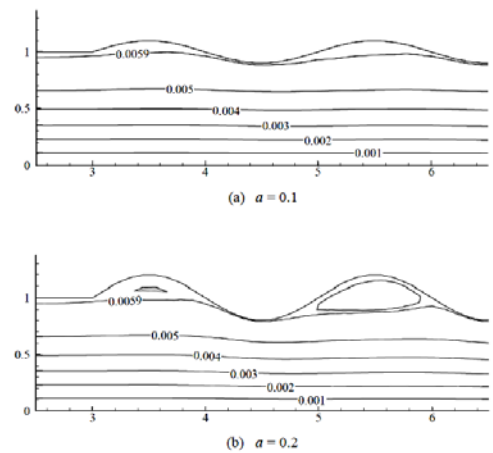


**Figure 17:** Wavy wall; Streamlines for Re = 500.

Distribution of  $ReC_f$  for the flow at Re = 500, for different amplitudes, is shown in Figure 16. The flow is a typical straight channel flow when  $a$  is zero. Thus the friction coefficient is constant. When the cross-sectional area is increased via increasing amplitudes, the fluid velocity at the corresponding cross-sectional area is reduced, thus reducing the friction coefficient,  $ReC_f$ . Recirculation zone occurs at top of the curve and becomes larger when the amplitude is increased as shown in Figure 17. In this area the values of  $ReC_f$  is negative.

Figure 18 presents the effects of changing Re for the flow with amplitude,  $a = 0.2$ . It is found that, the peak value of  $ReC_f$  for each wave is distinctly increased when the Reynolds number is increased, while the corresponding minimum value of  $ReC_f$  changes slightly. The velocity profiles at each location ( $3.5 \leq x \leq 8.5$ ) are presented in Figures 19 and 20. It is seen that a nearly fully-developed profile is attained at each wave bottom ( $x = 4.5, 6.5, 8.5$ ).

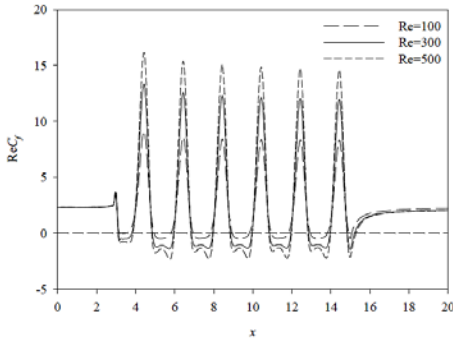


**Figure 18:** Wavy wall; Distribution of  $ReC_f$  with different Reynolds numbers for  $a = 0.2$ .

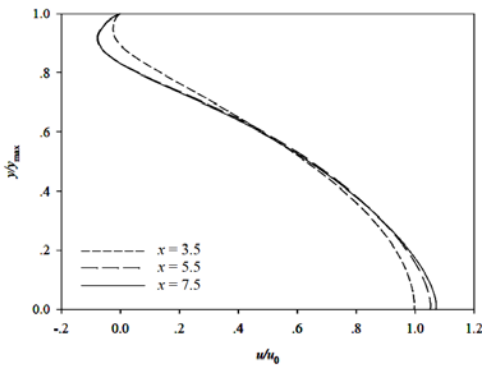


**Figure 19:** Wavy wall; Velocity profile at  $x = 3.5, 5.5$  and  $7.5$  ( $Re = 500$  and  $a = 0.2$ ).

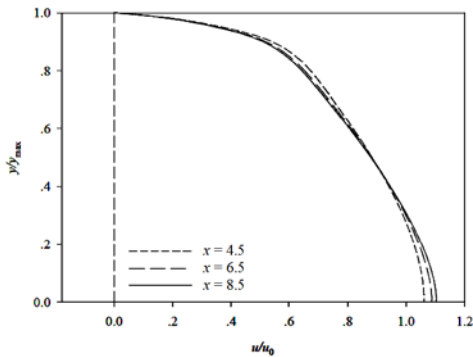


**Figure 20:** Wavy wall; Velocity profile at  $x = 4.5, 6.5$  and  $8.5$  ( $Re = 500$  and  $a = 0.2$ ).

## 6 Conclusions

A finite volume method with body-fitted coordinates is presented here. The grid is generated with the transfinite interpolation and then the grid smoothness is adjusted by the elliptic grid generation technique using Poisson equation. The governing equations in Cartesian coordinates are transformed into those in the body-fitted coordinate system via the chain rule and Jacobian matrix. A computer code is developed

and validated with analytical solution and available numerical data. The validated cases include heat conduction in a square plate with a hole, flow through a gradual-expansion channel and flow past a wavy wall channel.

The validation shows that the numerical results agree well with the published exact and numerical data. Thus, it may be concluded that the present computer code is adequate for calculation of such problems in complex domain.

## Nomenclature

$a$	Amplitude
$C_f$	Friction coefficient
$D$	Diameter
$I$	Maximum value of $\xi$
$J$	Maximum value of $\eta$ , Jacobian matrix
$k$	Thermal conductivity
$L$	Length of the domain
$m, n$	Number of data for calculation
$p$	Pressure
$P, Q$	Control function
$q$	Heat flux
$r$	Grid generation variable
$Re$	Reynolds number
$S$	Shape factor
$S_u, S_v$	Source term
$t$	Time
$T$	Temperature
$u, v$	Cartesian velocity components
$w$	Width of the domain
$x, y$	Cartesian coordinates
$y_w$	Channel height
$\phi, \psi$	Blending function
$\alpha, \beta, \gamma$	Geometric coefficients
$\xi, \eta$	Transformed body-fitted coordinates
$\mu$	Absolute viscosity
$\rho$	Density
$\tau$	Shear force
$\tau_w$	Skin friction

All dimensional variables are in SI units unless otherwise specified in the paper.

## References

- [1] Vinokur M., 1974. Conservation Equations of Gas Dynamics in Curvilinear Coordinate Systems, *Journal of Computational Physics*, 14: 105–125.
- [2] Thompson J.F., Thames F.C. and Mastin C.W., 1974. Automatic Numerical Generation of Body-fitted Curvilinear Coordinates System for Field Containing any Number of Arbitrary Two-dimensional Bodies, *Journal of Computational Physics*, 15: 299–319.
- [3] Thompson J.F., Thames F.C., Walker R.L. and Shanks S.P., 1975. Numerical Solutions of the Unsteady Navier-Stokes Equations for Arbitrary Bodies Using Boundary-Fitted Curvilinear Coordinates, *Magneto-hydrodynamics*, 485: 453–485.
- [4] Thompson J.F., 1982a. General Curvilinear Coordinate Systems, *Applied Mathematics and Computation*, 10–11: 1–30.
- [5] Thompson J.F., Warsi Z.U.A. and Mastin C.W., 1982b. Boundary-Fitted Coordinate Systems for Numerical Solution of Partial Differential Equations—A review, *Journal of Computational Physics*, 47: 1–108.
- [6] Gordon W.N. and Hall C.A., 1973. Construction of Curvilinear Coordinate Systems and Application to Mesh Generation, *International Journal of Numerical Methods in Engineering*, 7: 461–477.
- [7] Vanka S.P., Chen B.C. and Sha W.T., 1980. A Semi-Implicit Calculation Procedure for Flows Described in Boundary-Fitted Coordinate Systems, *Numerical Heat Transfer*, 3: 1–19.
- [8] Karki K.C., 1986. *A Calculation Procedure for Viscous Flows at All Speeds in Complex Geometries*, PhD Thesis, University of Minnesota.
- [9] Melaaen M.C., 1990. Analysis of Curvilinear Non-Orthogonal Coordinates for Numerical Calculation of Fluid Flow in Complex Geometries, *Doctoral Dissertation*, University of Trondheim.
- [10] Peric M., 1985. A Finite Volume Method for the Prediction of Three-Dimensional Fluid Flow in Complex Ducts, *PhD Thesis*, Imperial College London.
- [11] Shyy W., Tong S.S. and Correa S.M., 1985. Numerical Recirculating Flow Calculation Using a Body-Fitted Coordinate System, *Numerical Heat Transfer*, 8: 99–113.
- [12] Karki K.C. and Patankar S.V., 1989. Pressured Based Calculation Procedure for Viscous Flows at All Speeds in Arbitrary Configurations, *AIAA Journal*, 27(9): 1167–1174.
- [13] Talukdar P., Steven M., Issendorff F.V. and Trimis D., 2005. Finite Volume Method in 3-D Curvilinear Coordinates with Multiblocking Procedure for Radiative Transport Problems, *International Journal of Heat and Mass Transfer*, 48: 4657–4666.
- [14] Oztop H.F., 2005. Numerical Study of Flow and Heat Transfer in Curvilinear Ducts: Applications of Elliptic Grid Generation, *Applied Mathematics and Computation*, 168: 1449–1460.
- [15] Mohammed H.A., Gunnasegaran P. and Shuaib N.H., 2011. Numerical Simulation of Heat Transfer Enhancement in Wavy Microchannel Heat Sink, *International Communications in Heat and Mass Transfer*, 38: 63–68.
- [16] Piller M. and Stalio E., 2008. Compact Finite Volume Schemes on Boundary-Fitted Grids, *Journal of Computational Physics* 227: 4736–4762.
- [17] Baghlani A., 2012. Application of a High-Resolution Scheme in Simulation of Flow in Curved Channel Using Boundary-Fitted Curvilinear Coordinates, *Scientia Iranica A*, 19(6): 1463–1472.
- [18] Patankar S.V., 1980. Numerical Heat Transfer and Fluid Flow, *Hemisphere*.
- [19] Porameesanaporn J., 2006. Body-Fitted Finite Volume Method for Heat Conduction Problems, *Master Thesis*, Chulalongkorn University.
- [20] Putivisutisak S., 2006. A Finite Volume Method for Turbulent Flow in Complex Configuration Domains, *Report No. MRG4780188*, Thailand Research Fund (TRF).
- [21] Incropera F.P. and Dewitt D.P., 2002. *Fundamentals of Heat and Mass Transfer*, 5<sup>th</sup> ed., John Wiley and Sons.
- [22] Cliffe K.A., Jackson C.P. and Greenfield A.C., 1982. Finite Element Solutions for Flow in a Symmetric Channel with Smooth Expansion, *Technical Report AERE-R 10608*, Harwell Laboratory.
- [23] Burns A.D. and Wilkes N.S., 1987. A Finite Difference Method for the Computation of Fluid Flows in Complex Three Dimensional Geometries, *Technical Report AERE-R 12342*, Harwell Laboratory.
- [24] Wang C.C. and Chen C.K., 2002. Forced Convection in a Wavy-wall Channel, *International Journal of Heat and Mass Transfer*, 45: 2587–2595.